
Project: **SEAWave**

# Report on APD System for FR2-enabled Devices (MIMO/TAPD) Features (incl. Validation)

Work Package: WP 4

Deliverable: D4.2

Deliverable No.: D13

## Abstract

Deliverable No. 4.2 is the second deliverable of work package 4 (WP4) with the objective of developing a validated APD measurement system for mobile devices and laying the foundation for the experimental evaluation of FR2-enabled devices.
This report documents the completion of Deliverable 4.2. The measurement system for APD of FR2-enabled devices was successfully developed with a measurement uncertainty of $<$1.6 dB, validated within a normalized error $E_n$ of $\leq$0.5 and commercially released as DASY8 Module APD V1.0 by Schmid & Partner Engineering AG. The result, for the first time, enables FR2 devices to be tested with the novel APD safety limits.
The results of the work contributed to the IEC/IEEE TR 63572:2024 Technical Report on the "Evaluation of Absorbed Power Density Related to Human Exposure to Radio Frequency Fields From Wireless Communication Devices Operating Between 6 GHz and 300 GHz" as pre-stage to the product test standard IEC/IEEE pt63195-3 "Evaluation of Absorbed Power Density Related to Human Exposure to Radio Frequency Fields from Wireless Communication Devices Operating between 6 GHz and 300 GHz" that will include the developed methodology to test wireless device compliance with APD limits. In addition, the validation sources developed in this project by IT'IS and SPEAG will be used as test samples in the APD test round-robin as part of the finalization of IEC/IEEE TR 63572:2024. Systems have already been installed in the government laboratories of Japan and South Korea.

## Project Details

| | |
|---|---|
| Project name | SEAWave |
| Grant number | 101057622 |
| Start Date | 01 June 2022 |
| Duration | 36 months |
| Scientific coordinator | Prof. T. Samaras, Aristotle University of Thessaloniki (AUTH) |

# Deliverable Details

| | |
|---|---|
| Deliverable related number | D4.2 |
| Deliverable No. | D13 |
| Deliverable name | APD System for FR2-enabled Devices (MIMO/TAPD) Features (incl. Validation) |
| Work Package number | WP4 |
| Work Package name | Exposure Assessment of End User Devices |
| Editors | Sven Kuehn |
| Distribution | Public |
| Version | 1.0 |
| Draft / Final | Final |
| Keywords | FR2 Uplink Exposure |

# Contents

# 1 Introduction

To safeguard human health against the potential adverse effects of electromagnetic fields (EMFs), several international organizations have established safety guidelines. The International Commission on Non-Ionizing Radiation Protection (ICNIRP) and the IEEE International Committee on Electromagnetic Safety (IEEE ICES) provide such guidelines, which include basic restrictions (dosimetric limits) and reference levels (incident field limits) [1, 2].

The specific absorption rate (SAR), defined as the power absorbed per unit mass of tissue, has served as the dosimetric basic restriction to regulate electromagnetic exposure. This standard applies to frequencies up to 6 GHz [1] or 10 GHz [2], aiming to limit tissue heating to a maximum of $1^{\circ}$C. Established in the early 1970s [3], SAR has remained a cornerstone of safety guidelines. To support compliance, product standards have been developed to facilitate the assessment of peak spatial SAR values, particularly for transmitters operating within 2 mm of tissue simulation media [4].

The existing compliance framework for electromagnetic exposure proved adequate until the allocation of new frequency bands above 10 GHz for fifth-generation (5G) cellular network technology. These higher frequency bands were introduced to address the growing demand for faster data rates, more secure communication, and lower latency. However, adopting these bands has introduced novel human exposure scenarios, particularly near-field exposures in the millimeter-wave (mmW) range.

Initially, incident power density (IPD) [5] was employed as a pseudo-dosimetric limit. However, IPD does not account for near-field coupling or backscattering effects involving the human body, making it an inadequate metric for accurate exposure assessment [6]. To address these limitations, the most recent safety guidelines have introduced absorbed power density (APD) [1] or epithelial power density (PD) [2] as basic restrictions. These metrics are averaged over a square area of 4 $cm^2$ for frequencies between 6 – 30 GHz and 1 $cm^2$ for frequencies above 30 GHz, ensuring a more accurate limitation of maximum tissue heating.

## 1.1 State-of-the-Art

At the start of the project, the frequency range of commercial APD test systems was limited to 10 GHz to support testing in accordance with [7]. At frequencies above 10 GHz, only incident power density test systems were available to support product compliance testing in accordance with [8].

Four APD assessment methods have been proposed in the scientific literature [9]:

1. dosimetric probe method;
2. reflectivity-based phantom method;
3. thermal imaging;

4. over-the-air (OTA) augmented method.

The different methods come with specific advantages and disadvantages listed below:

| Method | Advantages | Disadvantages |
|---|---|---|
| dosimetric probe | • sensitivity sufficient for general public exposure limits<br>• accurate representation of the human skin (APD & reflection) | • lower measurement speed due to scanning |
| reflectivity-based phantom | • sensitivity sufficient for general public exposure limits<br>• suitable for frequencies $>$60 GHz | • scattering-only model **not valid in reactive near-field**<br>• **resolution limited** by waveguide probe dimension<br>• requires magnitude and phase |
| thermal imaging | • fastest method<br>• suitable for frequencies $>$60 GHz | • **sensitivity insufficient** for general public exposure limits<br>• published scattering models not valid in reactive near-field |
| over-the-air augmented | • versatile through digital twin principle | • **lacks** analytical / numerical / experimental **proof of concept** |

In summary, the dosimetric probe method developed in this project is the only suitable method for testing FR2 devices operated close to the human body. Its only drawback is a relatively slow assessment speed. All other methods show severe shortcomings in terms of use in reactive near-field or sensitivity restrictions.

## 1.2 Objective

WP4 will provide the necessary instrumentation, test, and validation procedures required to demonstrate compliance of FR2-enabled 5G devices with the latest safety guidelines [8], i.e., for (i) measuring APD, (ii) assessing the maximum exposure case for MIMO transmitters; (iii) demonstrating that the TAPD operates as indented in any device configuration. The results will be disseminated to the corresponding JWG-IEC/IEEE while SEAWave is still in progress in facilitating timely adoption by IEC/IEEE and later by CENELEC and the EU. In particular, D4.2's objective was to develop and validate an APD test system for FR2-enabled 5G devices.

# 2 APD Measurement System for Frequency Range 2

The Absorbed Power Density (APD) measurement system is designed to accurately emulate the reflection and absorption characteristics of electromagnetic waves in human skin. This system focuses on replicating the interaction of incident electromagnetic fields with the skin, including both the reflection and subsequent absorption of power within the tissue, which forms the basis for APD evaluation.

At the system's core is the skin model based on published human skin measurements data [10]. These measurements provide the essential parameters for defining the dielectric properties of human skin, ensuring that the model closely mirrors the real-world electromagnetic response of human tissue over age and gender variation. This includes variations in skin thickness, conductivity, and permittivity.

Based on the skin data, the APD system for the frequency range 2 was developed. Figure 1 details the system concept and the commercial DASY8 Module APD V1.2 system released in December 2024. Key elements are the

1. PHA-30G containing the SSL-30G skin emulating liquid;
2. EUAPDVx pseudo-vector E-field probe that allows the reconstruction of the APD inside the skin-simulating liquid.

Details of these components are outlined in the following sections.

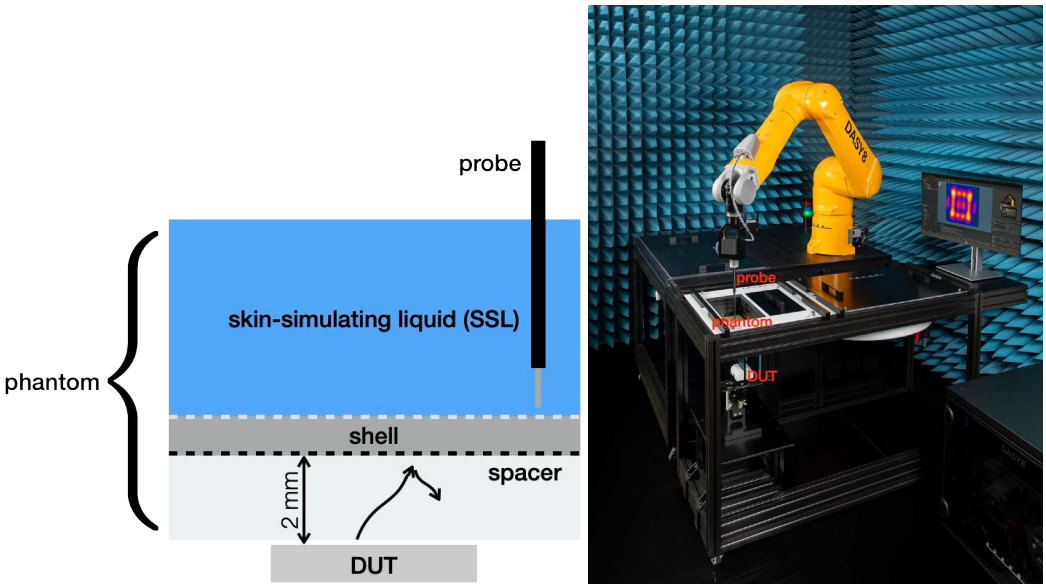


Figure 1: Left: Schematic of the APD measurement system based on the dosimetric probe principle. The skin-emulating phantom and skin-simulating liquid, the EUAPDVx pseudo-vector probe, and the device under test (DUT) under the phantom are shown. Right: Commercial implementation of the APD measurement system in DASY8 Module APD.

## 2.1 Skin Emulating Phantom

In Module APD, phantoms and skin-simulating liquids (SSL) form band-limited human skin APD and reflection coefficient mimicking phantoms. The phantoms were designed to emulate the reflection coefficient and the absorption in the human skin for reactive near-field conditions. To lower the measurement uncertainty of the dosimetric probe scanning the field inside the SSL, the phantoms and SSL were designed to generate a larger penetration depth in the SSL than in the real human skin. These optimization goals are achievable if the bandwidth of the phantom and SSL combinations can be limited. Therefore, SPEAG develops different phantom and SSL combinations for different frequency ranges. In WP4.2, the first phantom for FR2, which consists of the PHA-30G and SSL-30G, was developed.

### 2.1.1 PHA-30G and SSL-30G (24 - 30 GHz)

The PHA-30G (Figure 2) phantom and the SPEAG skin-simulating liquid SSL-30G reliably emulate the absorption and reflection characteristics of the human skin from 24 to 30 GHz. It enables the dosimetric evaluation of the APD of millimeter-wave devices in the 100 mm × 200 mm test area. A crosshair at the bottom of the phantom guides the positioning of devices under test below the phantom. A cover prevents evaporation of the liquid. Reference markings on the phantom allow the complete setup of all predefined phantom positions and measurement grids by teaching three points with the robot. During APD measurements, the phantom is filled with approximately 1 L of SSL-30G.

Figure 2: PHA-30G Phantom

## 2.2 EUAPDVx Probe

### 2.2.1 Probe Design

The *EUAPDVx* probe (Figure 3) utilizes a pseudo-vector design that not only measures the field magnitude but also derives its polarization ellipse. This design is advantageous because calibration can eliminate sensor angle errors and field distortions caused by the substrate and probe tip. This is particularly important in the operational frequency range of 10 GHz to 45 GHz, where field distortions due to the substrate and tip material are wavelength-dependent. Furthermore, the probe has been optimized for operation in the SSL, achieving minimal scattering and minimal deviation from an isotropic response to arbitrarily incident waves.

The probe consists of two orthogonal, electrically small resistive dipole sensors, each 1 mm in length, loaded with diode detectors. The low-frequency voltage signals from the detectors are transmitted via high-resistive lines, presenting a high impedance—thus ensuring transparency to radio-frequency electromagnetic fields. The probe has a diameter of 1.6 mm, and the sensor center is located 0.8 mm from the tip. The probe tip is made from a quartz cylinder filled with transparent epoxy that matches the probe's dielectric properties to the surrounding medium.


Figure 3: Left: Closeup photograph of the EUAPDDVx probe. Right: dimension of the probe tip and sensor location.

### 2.2.2 Probe Calibration

The probe calibration of EUAPDVx probes follows the two-step calibration process described in Appendix E3.2 of IEC/IECC 62209-1528. First, the sensitivity of the probe in air is calibrated using SPEAG's accredited 3-antenna calibration method in the frequency range from 10 GHz to 45 GHz. In addition, the dynamic range of the probe is linearized for

a large set of communication signals, including 5G NR FR2, using SPEAG's sensor model calibration (SMC). In the second step, the sensitivity in the specific SSL is determined by matching the analytically determined field distribution in the center of the calibration source with the probe's signal response (Figure 4).

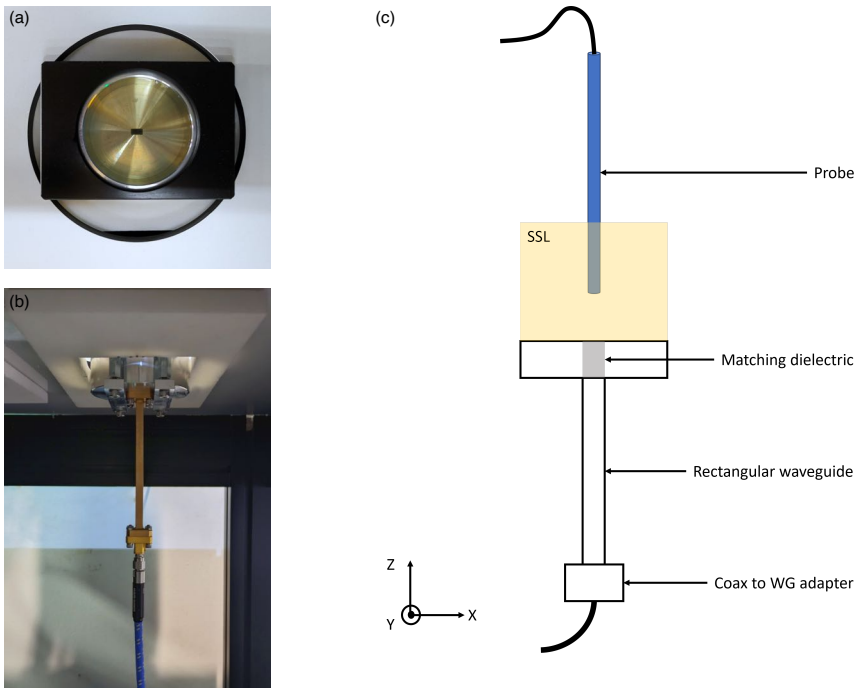


Figure 4: Second step (TSL) calibration setup for EUAPDVx probes covering the frequency range from 24 – 30 GHz with SSL30G. The setup consists of an open-ended waveguide with a dielectric matching layer radiating into a half-space of SSL. (a) top, and (b) side view of the implemented calibration source. (c) schematic of the calibration probes in the calibration source.

## 2.3 APD for MIMO

The developed APD test solution for MIMO-enabled devices builds upon and extends the advanced concepts and methodologies implemented in DASY8 Module mmWave:

1. Phase Reconstruction via Pseudo-Vector Measurement. The system leverages the ability to reconstruct the electromagnetic field phase from pseudo-vector measurements with the developed EUAPDVx probe inside the SSL [11]. This capability is critical for characterizing the complex vector field generated by MIMO transmitters. Combining amplitude and phase information enables the system to correlate the complex vector field distribution inside the SSL with the excitation configuration (also known as code-book) of the MIMO-enabled source. This is a critical capability to reduce the number of unknowns and hence the number of APD tests of MIMO-enabled devices.

2. The Maximum Exposure Optimizer (MEO) [12] is a pivotal feature in the APD test solution. MEO enables the reconstruction of the electromagnetic field for any potential MIMO source excitation configuration, provided that n+1 independent MIMO excitation configurations have been measured, where n is the number of antenna/source elements. This approach ensures that the system accounts for all possible excitation states, including the worst-case exposure scenarios, by intelligently extrapolating and optimizing the measured data.

This approach comprehensively addresses the unique challenges MIMO systems pose, where simultaneous multiple antenna/source elements dynamically influence exposure levels.

## 2.4 Time-average APD

### 2.4.1 Overview

The selected implementation of the APD measurement system for determining Time-Average APD (TAPD) leverages established methodologies and tools developed by P4, specifically those designed for the DASY8 Module mmWave and Module SAR (Figure 5). The APD solution builds on the dosimetric probe method, which has proven effective for accurate and reliable SAR measurements. By adapting the concepts from SAR, the APD measurement system ensures consistency with established workflows while addressing the unique challenges of devices with time-period power control.

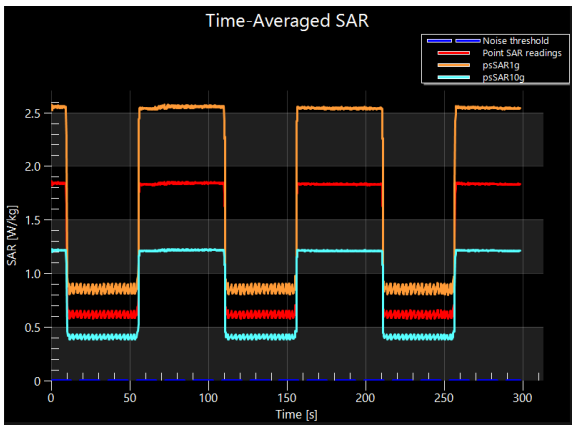


Figure 5: Implementation example of time-averaging in DASY8 Module SAR.

### 2.4.2 Time-average APD Implementation

The solution incorporates the workflow originally developed for SAR and described in the DASY8 System Handbook [13] in the chapter ”Workflow for Devices with Time Period Power Control.” In particular, the following work-flow is employed:

1. Assessment of the complex vector field distribution from the FR2-enabled devices inside the SSL as described in Section 2.3. (reference APD value)

2. Recording of the real-time evolution of the APD ($APD_{x,y,z,t}$) at a fixed location (x,y,t) with the EUAPDVx probe.
3. Scaling factor determination at every time sample determined in step 2.
4. Averaging of realtime APD distribution ($APD_{x,y,z,t}$) over the required averaging period.

Based on step 1 and 4 above the $T_x$ factor is determined as:

$$T_x = \frac{averageof APDreadings}{referenceAPDvalue} \tag{1}$$

Once the measurement is completed, the pAPD and psAPD are calculated in the DASY8 Module APD software:

$$\begin{aligned} TpAPD &= T_x \cdot pAPD \\ TpsAPD_{1cm^2} &= T_x \cdot psAPD_{1cm^2} \\ TpsAPD_{4cm^2} &= T_x \cdot psAPD_{4cm^2} \end{aligned} \tag{2}$$

With the above, the implementation of TAPD in our APD measurement solution provides a robust and reliable framework for evaluating exposure from modern wireless devices, including those with advanced power control and MIMO features.

## 2.5 APD Measurement System Uncertainty Budget

Measurement uncertainty is a critical factor in quantifying the accuracy and reliability of the APD measurement system. It ensures confidence in the results and provides a transparent framework for evaluating compliance with regulatory exposure limits. In the context of device type approval, accurately quantifying the uncertainty is essential to validate that devices meet the required safety standards under worst-case conditions.

For type approval of devices, regulators and manufacturers rely on standardized and well-documented measurement systems. The APD measurement system, developed under Task 4.2, is pivotal in this process. A clear understanding of the uncertainty budget ensures that the measurements and derived exposure limits are robust and defensible. This is particularly important given the increasing complexity of MIMO transmitters with TAPD features.

Within Task 4.2, the uncertainty budget of the APD measurement system was systematically determined. This process involved identifying and quantifying all significant sources of uncertainty across the system, including probe performance, calibration procedures, phantom, environmental factors, and repeatability. The results of this evaluation are summarized in Table 1, which presents the detailed uncertainty components and their contributions to the total measurement uncertainty. This analysis ensures that the APD measurement system adheres to the highest standards of precision and reliability.

# Uncertainty Budget

**APD Measurement System**

**(Frequency band: 24 –30 GHz range)**

| Sym-bol | Error Description | Uncert. value | Uncert. \|dB | Prob. Dist. | Div. | $c_i$ peak | $c_i$ 1 cm$^2$ | $c_i$ 4 cm$^2$ | Std. Unc. APD \|dB peak | 1 cm$^2$ | 4 cm$^2$ |
|---|---|---|---|---|---|---|---|---|---|---|---|
| **Measurement System** | | | | | | | | | | | |
| CF | Probe Calibration | 26.7 | 1.03 | N | 2 | 1 | 1 | 1 | 0.51 | 0.51 | 0.51 |
| $CF_{drift}$ | Probe Calib. Drift | 1.7 | 0.07 | R | 1.73 | 1 | 1 | 1 | 0.04 | 0.04 | 0.04 |
| LIN | Probe Linearity | 4.7 | 0.20 | R | 1.73 | 1 | 1 | 1 | 0.12 | 0.12 | 0.12 |
| BBS | Broadband Signal | 2.8 | 0.12 | R | 1.73 | 1 | 1 | 1 | 0.07 | 0.07 | 0.07 |
| ISO | Isotropy | 4.7 | 0.20 | R | 1.73 | 1 | 1 | 1 | 0.12 | 0.12 | 0.12 |
| DAE | Probe Electronics | 0.8 | 0.03 | N | 1 | 1 | 1 | 1 | 0.03 | 0.03 | 0.03 |
| AMB | RF Ambient | 1.0 | 0.04 | N | 1 | 1 | 1 | 1 | 0.04 | 0.04 | 0.04 |
| $\Delta$sys | Probe Positioning | ±0.1mm | 0.18 | N | 1 | 1 | 1 | 1 | 0.18 | 0.18 | 0.18 |
| PPS | Skin APD Reconstr. | 13.7 | 0.56 | R | 1.73 | 0.55 | 0.82 | 1 | 0.18 | 0.26 | 0.32 |
| **Phantom** | | | | | | | | | | | |
| SSL($\epsilon$) | SSL $\epsilon$ | 10.0 | 0.41 | R | 1.73 | 0.54 | 0.54 | 0.54 | 0.13 | 0.13 | 0.13 |
| SSL($\sigma$) | SSL $\sigma$ | 10.0 | 0.41 | R | 1.73 | 0.05 | 0.05 | 0.05 | 0.01 | 0.01 | 0.01 |
| DAK($\epsilon$) | SSL $\epsilon$ meas. | 3.2 | 0.14 | N | 2 | 0.54 | 0.54 | 0.54 | 0.04 | 0.04 | 0.04 |
| DAK($\sigma$) | SSL $\sigma$ meas | 5.2 | 0.22 | N | 2 | 0.05 | 0.05 | 0.05 | 0.01 | 0.01 | 0.01 |
| SSL($\epsilon$/T) | SSL $\epsilon$ on T | 1.2 | 0.05 | R | 1.73 | 0.54 | 0.54 | 0.54 | 0.02 | 0.02 | 0.02 |
| SSL($\sigma$/T) | SSL $\sigma$ on T | 5.1 | 0.22 | R | 1.73 | 0.05 | 0.05 | 0.05 | 0.01 | 0.01 | 0.01 |
| SHP | Shell Permittivity | 5.0 | 0.21 | R | 1.73 | 1.05 | 1.05 | 1.05 | 0.13 | 0.13 | 0.13 |
| SHT | Shell Thickness | 5.0 | 0.21 | R | 1.73 | 0.42 | 0.42 | 0.42 | 0.05 | 0.05 | 0.05 |
| SME(A) | Skin Emulation | 11.2 | 0.46 | R | 1.73 | 0.62 | 1 | 0.85 | 0.17 | 0.27 | 0.23 |
| SME(f) | Frequency Resp. | 5.6 | 0.24 | R | 1.73 | 1 | 1 | 1 | 0.14 | 0.14 | 0.14 |
| **Device** | | | | | | | | | | | |
| DIS | DUT to Pha. Dist. | 11.2 | 0.46 | R | 1.73 | 1 | 1 | 1 | 0.27 | 0.27 | 0.27 |
| H | Holder Effects | 0 | 0 | N | 1 | 1 | 1 | 1 | 0 | 0 | 0 |
| MOD | DUT Modulation | 9.7 | 0.4 | R | 1.73 | 1 | 1 | 1 | 0.23 | 0.23 | 0.23 |
| TAAPD | Time-average APD | 1.7 | 0.07 | R | 1.73 | 1 | 1 | 1 | 0.04 | 0.04 | 0.04 |
| RF drift | DUT Drift | 3.5 | 0.15 | N | 1 | 1 | 1 | 1 | 0.15 | 0.15 | 0.15 |
| **Corrections to the APD Results** | | | | | | | | | | | |
| C (R ) | APD scaling | 0.0 | 0.00 | R | 1.73 | 1 | 1 | 1 | 0.00 | 0.00 | 0.00 |
| u$\Delta$SAR | Combined Uncertainty | | | | | | | | 0.77 | 0.82 | 0.80 |
| U | **Expanded Uncertainty** | | | | | | | | **1.54** | **1.64** | **1.60** |

Table 1: Worst-case uncertainty budget for APD measurements of user devices and validation sources. The budget is valid for the frequency range 24 GHz–30 GHz and represents a worst-case analysis.

# 3 APD Validation

The objective of the validation is to ensure that the APD measurement system performs within the manufacturer's stated measurement uncertainty for any potential near-field source. The validation tests shall be "comprehensive", i.e., covering all potential exposure conditions (any antenna, any frequency, all near-field distances, etc.) and test all metrics, i.e., pAPD and the psAPD averaged over 1 $cm^2$ and 4 $cm^2$. This, for example, can be achieved by testing the envelope of the exposure conditions to reduce the number of tests dramatically. We developed a set of sources detailed in Section 3.3. We contributed the resulting sources to the IEC TC106 were they are currently used to perform a round-robin for APD measurement solutions as described in Section 1.1. The round-robin is planned to be completed in Q3 2025.

## 3.1 APD Validation Concept

The APD validation concept involves a two-step process to ensure the accuracy of the physical APD phantom implementation. First, the reflection coefficient of the phantom is validated against targets generated through full-wave simulations using the FDTD kernel in Sim4Life (ZMT ZurichMedTech AG, Switzerland). Second, the APD induced in the phantom is measured and compared with simulation results to verify that the phantom accurately replicates the absorption characteristics of human skin. These simulations were based on a target skin model derived from skin measurements reported [10]. To validate the reflection from the phantom, we simulate and measure the return loss of the validation sources broad-band, and apply cosine-similarity as a figure of merit. To validate the APD emulation, we compare the measured APD with the simulated target and test the agreement utilizing the normalized error $E_n$, a measure of how well the results agree within the combined simulation and measurement uncertainty.

## 3.2 APD Validation Sources

### 3.2.1 30 GHz Slot Array

The Horn Slot Array (HSA) is designed for system validation and consists of a pyramidal horn loaded with an array of rectangular slot antennas positioned on its aperture. The horn is fabricated from aluminum and plated with gold for enhanced performance. It employs a WR28 waveguide with a UG-599/U flange connected to a WR28 wideband waveguide adapter for feeding the slot array. To address the mismatch caused by loading the horn with the slot array, the slots have been optimized to achieve a typical return loss of better than 20 dB at the design frequency. The slots are symmetrically arranged on the horn's aperture and fabricated on a 0.15 mm thick metal sheet. This sheet is mounted to the pyramidal horn by soldering, ensuring robust and precise assembly.

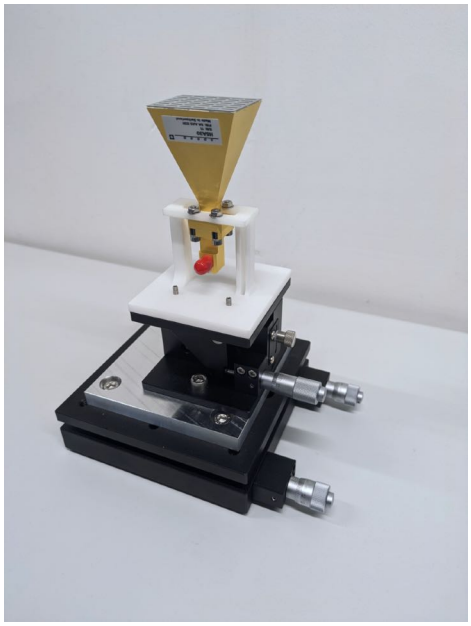

Figure 6: HSA30 (30 GHz slot array)

| Source | f /GHz | $P_{out}$ \|dBm |
|---|---|---|
| HSA30 | 30 | 10 |

Table 2: Nominal operational frequency and input power level to be applied to the 30 GHz slot array.

### 3.2.2 30 GHz Dipole Array

The Cavity-Fed Dipole Array (CDA) is an antenna design featuring dipoles printed on a low-loss dielectric substrate arranged in an offset lattice pattern determined by resonant cavity modes. These dipoles are excited via non-resonant slots located on the opposite side of the substrate, coupling energy from the cavity. The slots are located on the opposite face of the substrate as the dipoles. The resonant cavity generates the excitation modes, with energy introduced via a probe feed connected to a 2.92 mm coaxial connector.

Figure 7: CDA30 (30 GHz cavity-backed dipole array)

| Source | f /GHz | $P_{out}$ \|dBm |
|---|---|---|
| CDA30 | 30 | 13 |

Table 3: Nominal operational frequency and input power level to be applied to the 30 GHz dipole array

## 3.3 APD Validation Results

Figure 8 shows the similarity matrix of the simulated and measured reflection coefficients of the HSA30 validation source over distance. For the validation, the highest similarity has to fall into the diagonal of the matrix $\pm$ half a wavelength or 1.5 mm at 30 GHz. The results fall well into this requirement and, therefore, validate the reflection properties of the PHA-30G and SSL-30G phantom and liquid combination.

Table 4 summarizes the peak spatial average APD for 1 and 4 $cm^2$ of the horn slot array and cavity-backed dipole array, including associated numerical and experimental uncertainties and the results normalized errors (En) of the validation. The normalized errors are $<1$ for the validation cases and hence the system is also considered to be validated for APD assessments.

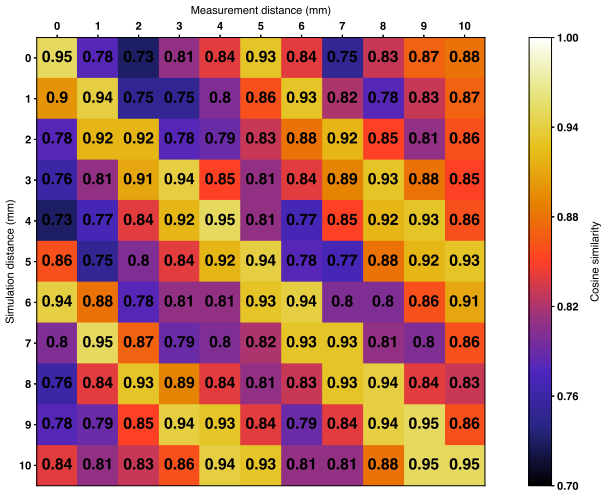


Figure 8: Similarity matrix of the simulated and measured reflection coefficients of the HSA30 validation source.

| Source | d /mm | signal | U meas \|dB | U sim \|dB | ΔpsAPD \|dB | | En | |
|---|---|---|---|---|---|---|---|---|
| | | | | | 1 $cm^2$ | 4 $cm^2$ | 1 $cm^2$ | 4 $cm^2$ |
| HSA | 2 | CW | 1.52 | 0.89 | 0.64 | 1.06 | 0.22 | 0.38 |
| CDA | 2 | CW | 1.52 | 1.17 | -0.87 | -1.05 | 0.23 | 0.28 |

Table 4: Peak spatial average APD validation results for 1 and 4 $cm^2$ of the horn slot array and cavity-backed dipole array including associated simulation (sim) and measurement (meas) uncertainties and the resulting normalized errors (En) of the validation

# 4 Conclusion

This report documents the completion of Deliverable 4.2. Task 4.2 successfully delivered a commercially released APD measurement system (DASY8 Module APD) that meets the highest standards for accuracy and reliability. The system accurately emulates the absorption and reflection properties of human skin in the mmWave frequency range of 24–30 GHz. The system was comprehensively validated using sources representative of near-field exposure from mobile devices operating in the FR2 frequency range, achieving a normalized error or normalized deviation well below 1. Furthermore, the system fulfills the requirements for type approval of commercial wireless products, including advanced features such as time-averaged exposure mitigation strategies and support for MIMO technologies. Systems have already been installed in the government laboratories of Japan and South Korea.

# Bibliography


[1] International Commission on Non-Ionizing Radiation Protection et al. 'Guidelines for limiting exposure to electromagnetic fields (100 kHz to 300 GHz)'. In: *Health physics* 118.5 (2020), pp. 483–524.

[2] IEEE. 'IEEE standard for safety levels with respect to human exposure to electric, magnetic, and electromagnetic fields, 0 Hz to 300 GHz'. In: *IEEE Std.* (2019).

[3] Niels Kuster and Quirino Balzano. 'Experimental and numerical dosimetry'. In: *Mobile Communications Safety*. Ed. by Niels Kuster, Quirino Balzano and James C. Lin. Boston, MA: Springer US, 1997, pp. 13–64. ISBN: 978-1-4613-1205-5. DOI: 10.1007/978-1-4613-1205-5_2. URL: https://doi.org/10.1007/978-1-4613-1205-5_2.

[4] IEC/IEEE 62209-1528. *Measurement Procedure for the Assessment of Specific Absorption Rate of Human Exposure to Radio Frequency Fields From Hand-Held and Body-Worn Wireless Communication Devices—Human Models, Instrumentation and Procedures (Frequency Range of 4 MHz to 10 GHz)*. International Electrotechnical Commission Geneva, Switzerland, 2020.

[5] International Commission on Non-Ionizing Radiation Protection et al. 'Guidelines for limiting exposure to time-varying electric, magnetic, and electromagnetic fields (up to 300 GHz)'. In: *Health physics* 74.4 (1998), pp. 494–522.

[6] Andreas Christ et al. 'Limitations of incident power density as a proxy for induced electromagnetic fields'. In: *Bioelectromagnetics* 41.5 (2020), pp. 348–359.

[7] IEC 63446 PAS. *Conversion method of specific absorption rate to absorbed power density for the assessment of human exposure to radio frequency electromagnetic fields from wireless devices in close proximity to the head and body – Frequency range of 6 GHz to 10 GHz*. Geneva, Switzerland: International Electrotechnical Commission (IEC), IEC Technical Committee 106, 2022.

[8] IEC/IEEE 63195-1. *DRAFT Assessment of power density of human exposure to radio frequency fields from wireless devices in close proximity to the head and body (Frequency range of 6 GHz to 300 GHz) - Part 1: Measurement procedure*. Geneva, Switzerland: International Electrotechnical Commission (IEC), IEC Technical Committee 106, 2022.

[9] IEC/IEEE TR 63572 ED1. *Evaluation of absorbed power density related to human exposure to radio frequency fields from wireless communication devices operating between 6 GHz and 300*. Geneva, Switzerland: International Electrotechnical Commission (IEC), IEC Technical Committee 106, 2024.

[10] Andreas Christ et al. 'Reflection properties of the human skin from 40 to 110 GHz: A confirmation study'. en. In: *Bioelectromagnetics* 42.7 (Oct. 2021), pp. 562–574. DOI: 10.1002/bem.22362. URL: https://www.mendeley.com/catalogue/adec553a-00f2-3c85-be8c-8f4cbe5e857f/?utm_source=desktop&utm_medium=1.19.8&utm_campaign=open_catalog&userDocumentId=%7B61612fd0-34a0-4948-b7e2-8cfa33434086%7D.

[11] Serge Pfeifer et al. 'Total Field Reconstruction in the Near Field Using Pseudo-Vector $E$-Field Measurements'. In: *IEEE Transactions on Electromagnetic Compatibility* 61.2 (2019), pp. 476–486. DOI: 10.1109/TEMC.2018.2837897.

[12] Sylvain Reboux et al. 'Fast method for exposure assessment of beam-forming millimeter-wave devices'. en. In: *Abstract collection of XXXIV General Assembly and Scientific Symposium (GASS) of the International Union of Radio Science (Union Radio Scientifique Internationale-URSI),* URSi GASS 2021, Aug. 2021, p. 1.

[13] Schmid & Partner Engineering AG. *DASY8 Module SAR System Handbook*. May 2025. URL: https://speag.swiss/downloads/.